NANO LETTERS

Letter

pubs.acs.org/NanoLett

Giant Current-Perpendicular-to-Plane Magnetoresistance in Multilayer Graphene as Grown on Nickel

S. C. Bodepudi, A. P. Singh, and S. Pramanik*

Department of Electrical and Computer Engineering, University of Alberta, Edmonton, Alberta T6G 2V4, Canada

Supporting Information

ABSTRACT: Strong magnetoresistance effects are often observed in ferromagnet−nonmagnet multilayers, which are exploited in state-of-the-art magnetic field sensing and data storage technologies. In this work we report a novel current-perpendicular-to-plane magnetoresistance effect in multilayer graphene as grown on a catalytic nickel surface by chemical vapor deposition. A negative magnetoresistance effect of ~10^4% has been observed, which persists even at room temperature. This effect is correlated with the shape of the 2*D* peak as well as with the occurrence of *D* peak in the Raman spectrum of the as-grown multilayer graphene. The observed magnetoresistance is extremely high as compared to other known materials systems for similar temperature and field range and can be qualitatively explained within the framework of "interlayer magnetoresistance" (ILMR).

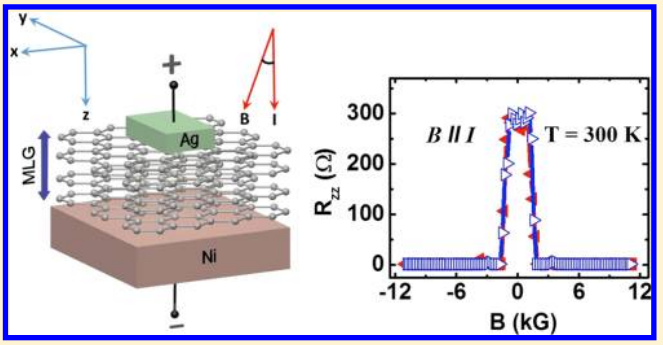

KEYWORDS: *Graphene, chemical vapor deposition, Raman spectroscopy, interlayer magnetoresistance, current-perpendicular-to-plane transport*

Artificial layered structures often exhibit strong magnetoresistance (MR) effects that are exploited in various data storage and magnetic field sensing technologies.[1] Graphite is a naturally occurring layered material in which single graphitic layers (or "graphene") are stacked on each other. Graphene, epitaxially grown on ferromagnets (such as nickel), is particularly attractive for spintronics because such systems can potentially realize perfect spin filtering[2] and giant Rashba splitting.[3] However, CPP (current-perpendicular-to-plane) MR properties of such layered graphene/ferromagnet structures are still largely underexplored. Here we consider multilayer graphene (MLG) as grown on nickel by chemical vapor deposition (CVD) and show that these structures exhibit large and nearly temperature-independent CPP-MR of ~10^4% for a small magnetic field of ~2 kilogauss. This MR effect is correlated with the shape of the 2*D* peak and also with the occurrence of the *D* peak in Raman spectrum of as-grown MLG. These Raman features can be controlled by varying the CVD growth parameters. Such a large negative CPP-MR, which persists even at room temperature, has hitherto not been reported in any graphitic system.[4−14]

Figure 1a shows the device schematic. CVD growth of MLG is performed on 2 cm × 2 cm nickel (Ni) foils, which act as catalyst for graphene growth as well as bottom electrical contact. To ensure uniform current distribution,[6] the second contact is fabricated at the center of the top MLG surface using silver epoxy. The area of the top contact is ~1 mm^2. As shown in Figure S1 (section I, Supporting Information), the Ni substrate is polycrystalline with primarily (111) grains. Details of the fabrication process are provided in section I of Supporting Information.

Figure 1b shows a FESEM image of the as-grown large-area MLG on Ni. Raman spectra taken from three representative regions of this sample are shown in the top inset of Figure 1b. The top Raman spectrum (black line) is most commonly observed, with few occurrences of the other two (blue and red). The strong *G* peak (~1580 cm^{-1}) indicates the formation of hexagonal lattice of carbon atoms. The absence of disorder-induced *D* peak (~1360 cm^{-1}) indicates extremely low density of defects. We note that no *D* peak has been found in any area of the sample. The 2*D* peak (~2700 cm^{-1}) is weaker compared to the *G* peak and has a wide line width of ~50 cm^{-1}, and its position is slightly upshifted compared to single layer graphene.[15] These features indicate the presence of multiple graphene layers,[15−17] which has been independently confirmed by transferring the MLG on SiO_2/Si substrate[15,18] (section II, Supporting Information). The average thickness of MLG has been found to be ~200 nm (Figure S2).

Unlike HOPG (highly oriented pyrolytic graphite), the 2*D* line shape of the as-grown MLG samples does not exhibit any clear "shoulder" peak at the lower frequency side of the 2*D* band or any pronounced "splitting" (Figure 1b). Such an absence of "shoulder" peak and splitting has been observed before in CVD-grown MLGs and turbostratic graphite.[15,16,19,20]

Received: August 17, 2013
Revised: March 22, 2014

dx.doi.org/10.1021/nl4030853 | *Nano Lett.* XXXX, XXX, XXX−XXX

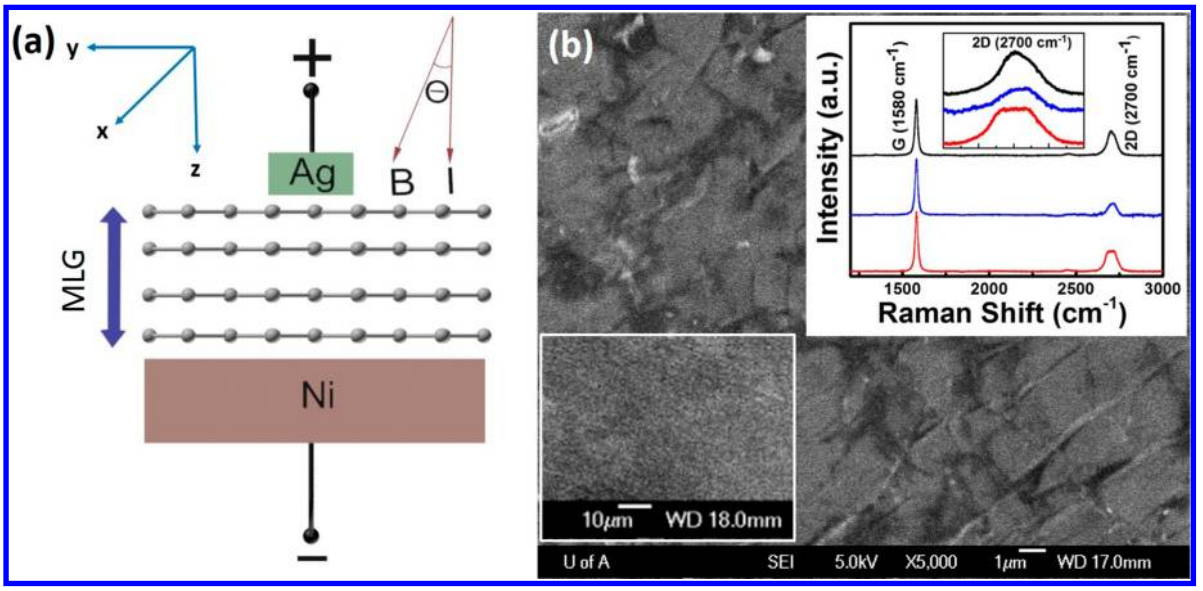

Figure 1. Device schematic and Raman characterization. (a) Measurement geometry. The MLG (*xy* plane) is grown on the bottom Ni substrate by CVD. CPP resistance R_{zz} is measured between Ag and Ni contacts. (b) Field emission scanning electron microscopic (FESEM) image of as-grown MLG on Ni. Bottom inset shows the bare Ni surface. The Raman spectra (top inset) have been taken from three representative areas of the as-grown sample. The 2*D* bands do not show HOPG-like "shoulder" peak or any significant splitting. The *D* peak is not present anywhere. The top Raman spectrum (black line) is most commonly observed, with few occurrences of the other two (blue and red).

However, such features appear after transferring the MLG on SiO_2/Si substrate (Figure S2).

We note that the typical penetration depth of Raman laser into graphite is ∼50−100 nm,[21−24] and hence the Raman data in Figure 1b conveys information about the graphene layers away from Ni/MLG interface. These layers are free from any crystal defect as evidenced by the absence of Raman *D* peak mentioned above. As described later, thinner MLG specimens exhibit a Raman *D* peak that originates from the defects at the Ni/MLG interface and the layers close to the interface. Thus, the as-grown MLG on Ni has two distinct regions: (a) Ni/MLG interface and layers close to this interface ("defective region") and (b) layers away from Ni/MLG interface ("defect-free region").

Figure 2 shows the magnetic field (B) dependence of the "current-perpendicular-to-plane" (CPP) resistance (R_{zz}) at various temperatures (T). CPP-MR depends strongly on the direction of the magnetic field. For "B in plane" geometry ($B \perp I$ or, $\theta = \pi/2$ in Figure 1a), a weak positive MR of ∼3% or less is observed (insets of Figure 2), which gradually becomes weaker as the temperature is increased. Here magnetoresistance (MR) is defined as $[R_{zz}(11\ \text{kG}) - R_{zz}(0\ G)] \times 100\%/R_{zz}(11\ \text{kG})$. However, in "$B$ normal to plane" geometry ($B \parallel I$ or, $\theta = 0$ in Figure 1a), resistance decreases drastically as B is increased, and this negative MR persists over the entire temperature range of 10−300 K. We note that the amount of resistance change is extremely large, ∼2 orders of magnitude over a moderate field range of ∼2 kG. Semiclassical models do not predict such effects since Lorentz force on charge carriers is zero in $B \parallel I$ configuration. Multiple devices (∼30) have been tested and large resistance change (minimum by a factor of 2, i.e., MR ∼ 10^2%) has been recorded in most cases (∼20).[25]

To gain further insight into CPP charge transport, we have performed temperature and magnetic field dependent current−voltage (I−V) measurements on the devices reported in Figure 2. Previous works have modeled CPP transport as a combination of in-plane (xy) charge transport in constituent layers and phonon- or impurity-assisted interlayer (z) charge transfer.[12,26,27] For a disorder-free system, the latter exhibits insulator-like temperature dependence ($dR_{zz}/dT < 0$).[26,27] In-plane resistance ($R_{\text{in-plane}}$), on the other hand, has a metal-like temperature dependence ($dR_{\text{in-plane}}/dT > 0$).[26,27] However, recently it has been shown that in-plane resistance of CVD-grown graphene can also exhibit insulator-like temperature dependence.[28] As shown in Figure 3a, we observe an insulating behavior of the CPP resistance in our samples. In-plane resistance in our samples also exhibits insulating behavior (Supporting Information, Section III), which is consistent with ref 28. However, in-plane resistance does not show any strong negative MR effect in the presence of an out-of-plane magnetic field. Instead, it only shows a weak positive MR effect (Supporting Information, Figure S3), which is consistent with previous studies.[13] In-plane transport in graphene nanoribbons can lead to large negative MR in the presence of an out-of-plane magnetic field.[29−31] However, this effect occurs over a field range of several teslas and is qualitatively different than the MR effects reported in Figure 2. Thus, the in-plane charge transport component is not dominant in the measured CPP resistance, and the large negative MR observed in Figure 2 must originate from interlayer charge transport (along $\hat{z}$) between the graphene layers. We note that the insulating behavior of CPP resistance (or R_{zz}) in Figure 2 persists both under zero field and high field conditions (Figure 3a), which excludes "magnetic field induced metal-insulator transition"[6] as the possible mechanism behind the observed large CPP-MR effect. Reference 6 reported a positive MR in graphitic samples, which is associated with the metal−insulator transition. Here, on the other hand, we observe a negative MR, and our devices remain insulating over the measured magnetic field range (Figure 3a).

The current−voltage (I−V) characteristics are linear (Figure 3b) over a bias range of [−1 mV, 1 mV], which indicates that CPP-MR is independent of bias at least in ±1 mV range. The zero-field I−V characteristics are also linear in this bias range as shown in Figure S4 (Supporting Information). Thus, "magnetic

dx.doi.org/10.1021/nl4030853 | Nano Lett. XXXX, XXX, XXX−XXX

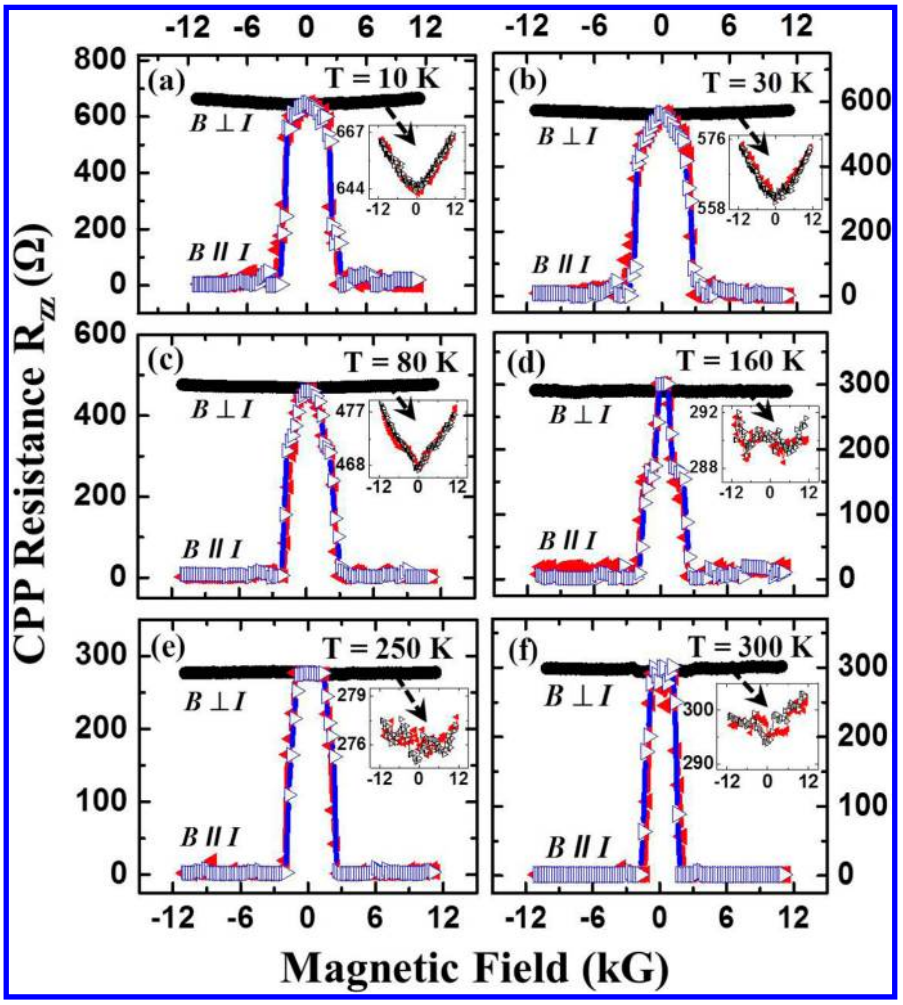

Figure 2. Magnetic field dependence of CPP resistance R_{zz} in the temperature range 10−300 K for MLG/Ni samples. For each temperature two orientations of the magnetic field have been considered: (i) $B \parallel I$ ($\theta = 0$) and (ii) $B \perp I$ ($\theta = \pi/2$). Giant negative magnetoresistance is observed in $B \parallel I$ configuration, whereas in $B \perp I$ geometry weak positive magnetoresistance is recorded (insets), which becomes less pronounced at higher temperatures. Both scan directions are shown in each plot, indicating the absence of any hysteresis. Each resistance value is the average of 50 readings. For $B \parallel I$, minimum resistance (occurring at high fields) is ∼2−4 Ω as shown later in Figure 3a. In all cases, bias current is 1 mA dc.

field induced shifting of current path" appears to be an unlikely mechanism behind the observed MR effect. Further, as mentioned before such mechanism is virtually ineffective in the $B \parallel I$ geometry due to the absence of Lorentz force. This mechanism is strongest in the $B \perp I$ geometry, but we have observed significantly weaker MR in this case (Figure 2, insets). We note that similar linear $I-V$ characteristics have been reported before for c-axis transport in multilayer graphene stacks.[12] Resistance values measured at a higher current bias (1 mA, Figures 2, 3a) match reasonably well with the slopes of the $I-V$ curves in Figures 3b, S4. Thus, it appears that the linearity of the $I-V$ curves is maintained over a relatively wide current bias of 1 mA. We avoid applying even larger bias in order to prevent sample damage due to large out-of-plane electric field in the CPP geometry.

To explore the role of the Ni/MLG interface and nearby graphene layers, we have studied Ni-grown MLG samples, in which the thickness of MLG is ∼15−20 nm (Figure 3c, d). CVD growth conditions have been kept the same as before (section I, Supporting Information). Smaller thickness of Ni substrate (∼600 nm, e-beam evaporated) has been used in this case to obtain thinner MLG. These thinner specimens show a pronounced defective (D) peak in the Raman spectrum (Figure 3c), which was not present in the thicker samples (Figure 1b). This is expected since it is well-known that layers close to the Ni surface do not resemble graphene-like behavior due to strong overlap between 3d states of Ni and 2p_z states of carbon.[32] For example, these interfacial layers have been known to exhibit a band gap, a presence of electronic states in the band gap and an absence of Dirac point.[32] Layers grown on top of these defective layers are expected to contain defects as well, which is consistent with the Raman data in Figure 3c.

We have only observed a very weak positive CPP-MR (∼0.3%) response from this "defective region" (Figure 3d). This indicates that the large negative CPP-MR effect reported in Figure 2 does not directly originate from the "defective region" close to the Ni/MLG interface. The "defective region" also exhibits weak metallic temperature dependence of CPP resistance (Figure 3d), which is opposite of what is observed in the thicker specimens (Figure 3a). The resistance of Ni contact itself is ∼1% of overall CPP resistance, and it does not exhibit any measurable MR (Figure S5, Supporting Information). All of these evidence indicate that the transport behavior in Figures 2 and 3a,b is not limited by the "defective region" in the vicinity of Ni/MLG interface but is governed by the "defect-free region" located away from the Ni/MLG interface. In section III

dx.doi.org/10.1021/nl4030853 | Nano Lett. XXXX, XXX, XXX−XXX

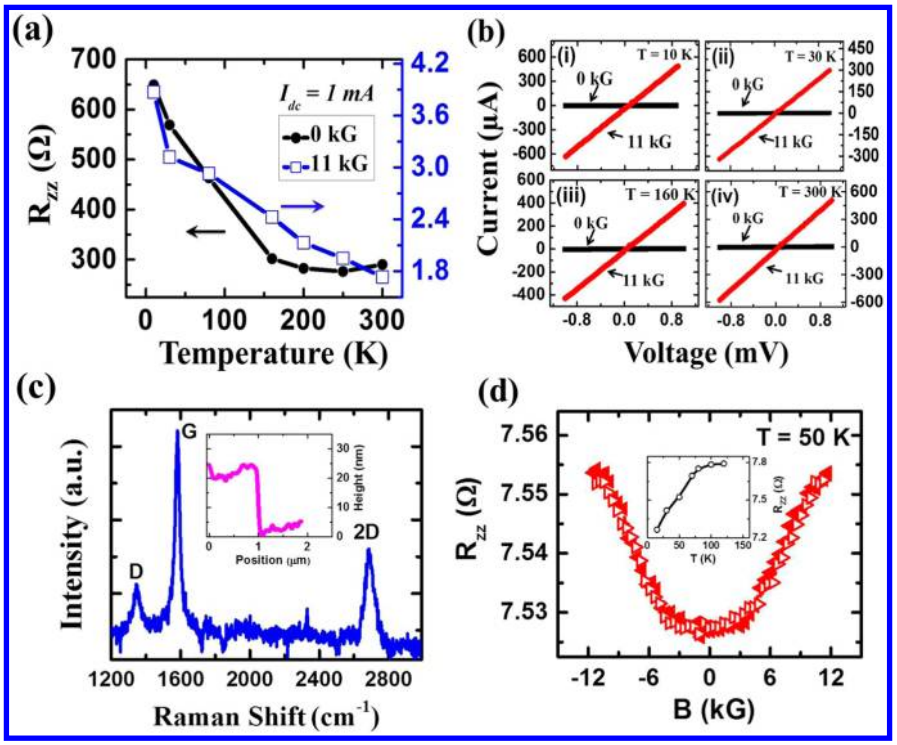

Figure 3. CPP charge transport characteristics of thicker samples and control experiments on thinner specimens. (a) $R_{zz}(T)$ at zero field and high field indicate insulating behavior and absence of any field induced metal−insulator transition in thicker (∼200 nm) samples. (b) $I-V$ characteristics of thicker samples at four different temperatures, indicating bias independence of the CPP-MR in ±1 mV range. For zero magnetic field, current ∼ few μA at 1 mV bias. A zoomed-in image of the zero-field $I-V$ data is shown in the Supporting Information, section IV. (c) Raman spectrum of thinner (∼15−20 nm) MLG samples as grown on Ni, which shows a defect (D) peak, and the inset shows typical step-height measurement. (d) Weak positive CPP-MR and metallic temperature dependence of CPP resistance R_{zz} (inset) of these thinner samples.

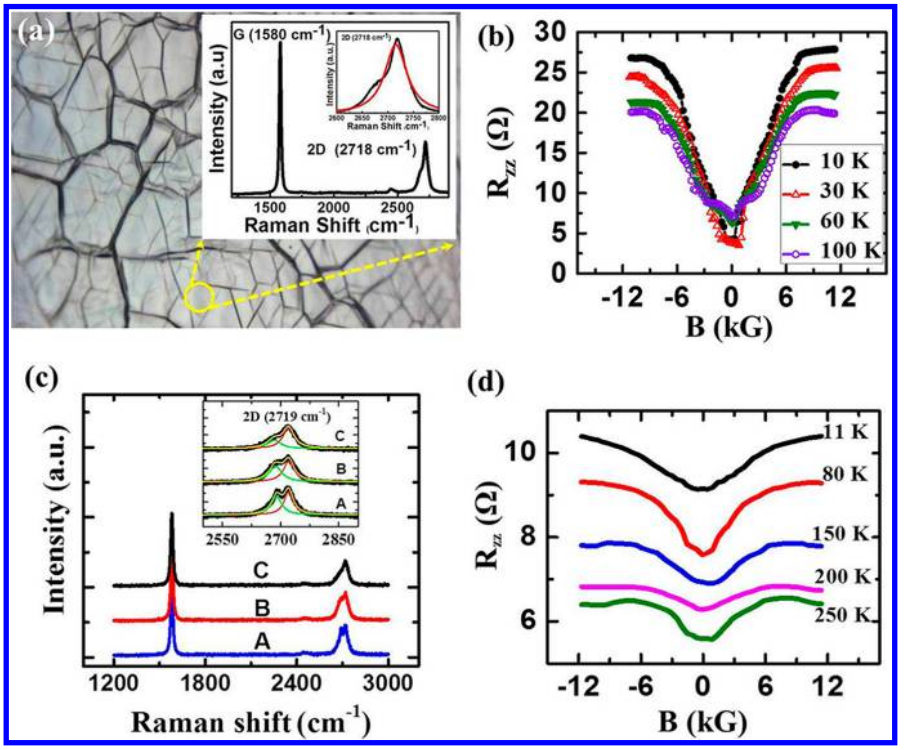

Figure 4. Raman and CPP-MR characterization of control devices (CVD-grown MLG-on-Ni—case of distorted 2D bands). (a) The 2D peak in the Raman signal shows a HOPG-like shoulder peak (inset). (b) R_{zz} vs B in the $B \parallel I$ geometry. A metal−insulator transition is observed near ∼1 kG. (c, d) Raman characteristics and CPP-MR of commercial MLG/Ni samples (from Graphene Supermarket). The 2D band in the Raman spectra is clearly distorted, and no negative CPP-MR has been observed.

dx.doi.org/10.1021/nl4030853 | *Nano Lett.* XXXX, XXX, XXX−XXX

of the Supporting Information we have shown that MLG/Ag paste contact resistance does not play any role either in the observed large negative CPP-MR.

To our knowledge, CPP-MR of as-grown MLG on Ni has not been studied previously, and the large negative CPP-MR observed in Figure 2 has not been reported before in any graphene-based system. However, growth on Ni substrate alone is not sufficient for observation of the large negative CPP-MR effect. As described above, this effect is absent in MLG that exhibits a Raman *D* peak. The negative CPP-MR originates from the "defect-free region" away from the Ni/MLG interface and has been found to be correlated with the 2*D* line shape in the Raman spectrum of the "defect-free region". As mentioned before, the devices characterized in Figures 1 and 2 do not exhibit any significant splitting or HOPG-like shoulder peak in the 2*D* Raman band, and a large negative CPP-MR is observed in these samples. We have grown MLG samples of similar thickness (~200 nm, on Ni) that exhibit HOPG-like shoulder peak in the Raman 2*D* band of the "defect-free region" (Figure 4a), by controlling the CH_4:H_2 ratio during CVD.[33] Such samples have not shown any negative CPP-MR but showed positive CPP-MR instead, with magnetic field-dependent metal−insulator transition (Figure 4b). These features are consistent with prior CPP measurements performed on HOPG.[6] Further, we have performed CPP measurements on commercially available thick (~100 nm) MLG on Ni (Graphene Supermarket). The 2*D* Raman bands from the "defect-free region" of these samples exhibit pronounced splitting (Figure 4c), and these samples show no large negative CPP-MR (Figure 4d). Thus, we conclude that the large negative CPP-MR originates from the graphene layers that are free of crystal defects (Raman *D* band is absent) and that are characterized by a distortion-free 2*D* Raman band. The thinner specimens (Figure 3c, d) show a distortion-free Raman 2*D* band, but it is accompanied by a Raman *D* band, and no large negative CPP-MR has been observed in this case.

Negative MR in the vicinity of zero magnetic field can originate from three sources: (a) weak localization,[12] (b) spin filtering and associated giant magnetoresistance (GMR) effect,[2] and (c) interlayer tunneling between zero mode Landau levels.[34−37] Negative MR originating from weak localization gradually diminishes with increasing temperature due to the reduction of phase coherence time at higher temperatures.[12] In our MLG/Ni samples (Figure 2), however, the negative MR is relatively insensitive to temperature. Additionally, the shape and angle dependence of MR in Figure 2 are qualitatively different than that observed in the case of weak localization, and for thick samples such as ours this effect is not expected to occur.[12] Finally, the negative MR effects shown in Figure 2 are orders of magnitude stronger than a typical weak localization related effect in a similar system.[12] Therefore, it is unlikely that the MR response shown in Figure 2 originates from weak localization.

Very recently a novel "perfect spin filtering" effect has been proposed in MLG CVD-grown on (111) Ni.[2] Due to the very high degree of spin filtering (~100%), such an effect can give rise to very large negative MR. According to this theory, perfect spin filtering is achieved due to special energy band alignment at (111) nickel/graphene interface, which promotes transmission of *only* minority spins through the graphene.[2] The presence of multiple graphene layers (3−4 or more) quenches any tunneling conductance of majority spins. However, in our case such spin-dependent transport cannot be used to explain the observed MR. This is because our device (Ni/MLG/Ag) is *not* a "spin valve" type device since the top electrode (Ag) is *nonmagnetic*. Thus, unlike ferromagnetic contacts, this electrode is not able to differentiate between various spin orientations. Thus, we believe that the observed large MR in Figure 2 is *not* due to this spin filtering effect.

Negative MR can also arise from an interlayer tunneling mechanism, which is often dubbed "interlayer magnetoresistance" or ILMR.[34−37] This effect is observed in a stack of two-dimensional (2D) massless Dirac electron systems. The interlayer coupling between these 2D layers should be sufficiently weak so that the entire system can be viewed as a stack of 2D systems instead of a bulk 3D material. In such systems out-of-plane charge transport occurs via interlayer tunneling. Such interlayer current can be tuned by a large factor by applying an out-of-plane magnetic field. The physical origin of this ILMR effect is described below.

For a stack of weakly coupled 2D massless Dirac electron system in absence of any magnetic field, electronic dispersion of each layer can be modeled by a linear $E-k$ spectrum (or "Dirac cone dispersion") with Fermi level located at the Dirac points.[38] The density of states (DOS) is small at the vicinity of the Dirac point, since it depends linearly on energy measured from the Dirac point.[38] When an out-of-plane electrical bias is applied, carriers tunnel from one layer to the next. In this case small tunneling current is expected due to low DOS near the (quasi) Fermi level of each layer.

When an out-of-plane magnetic field is applied, the linear $E-k$ dispersion of each layer converts into a series of Landau levels, with a (zero mode) Landau level located at the Dirac point.[38] Out-of-plane charge transport will now occur via interlayer tunneling between the zero mode Landau levels. The degeneracy of the Landau levels increases with magnetic field. Thus, with an increasing magnetic field, the degeneracy of the zero mode Landau level will increase, giving rise to a larger interlayer tunneling current. This is the origin of large negative MR and is dubbed ILMR.[34−37]

If the magnetic field is in-plane, it exerts a Lorentz force on the electrons traveling out-of-plane and bends their trajectories. As a result, with an increasing in-plane magnetic field, the effective interlayer tunneling distance increases, resulting in weaker tunneling probability and hence a smaller interlayer tunneling current. Thus, a weak positive MR is observed when the magnetic field is in-plane.

The stack of two-dimensional massless Dirac electron systems can be realized by stacking multiple graphene layers provided the interlayer coupling is sufficiently weak. Further, in order to observe the above-mentioned effect, one has to ensure that out-of-plane charge transport occurs primarily via interlayer tunneling and not via some conductive defect states electrically shorting neighboring graphene layers. As described below, in our devices (Figures 1 and 2), both of these conditions are fulfilled by the graphene layers in the "defect-free region" (i.e., layers away from the Ni/MLG interface).

We note that the lack of pronounced splitting (or lack of HOPG-like "shoulder peak") in the 2*D* band of the Raman spectrum (Figure 1b) indicates weak interlayer coupling in the "defect-free region" of these samples. The 2*D* band in the Raman spectrum of (monolayer) graphene originates due to a second order, two-phonon, "double resonance" process, which has been analyzed extensively by various theoretical and experimental techniques.[16,39−43] Briefly, in this process first an electron−hole pair is created around the K valley by a laser

dx.doi.org/10.1021/nl4030853 | *Nano Lett.* XXXX, XXX, XXX−XXX

photon. Next, the electron is scattered by a (iTO) phonon to the K′ valley. Then the electron is scattered back to the K valley by another iTO phonon. This electron then recombines with a hole and emits a photon. For monolayer graphene this process leads to a single Lorentzian 2*D* peak in the Raman spectrum. Now, for bilayer/trilayer graphene or graphite the single electronic dispersion curve of monolayer graphene is split into multiple branches due to interlayer coupling.[38] As a result above-mentioned double-resonance scattering processes can take place between various branches, resulting in multiple slightly shifted Lorentzian peaks. The resultant 2*D* band is a combination of all of these Lorentzians and therefore loses its symmetrical shape and shows signs of splitting and distortion. In particular, for bilayer graphene four double-resonance processes can occur resulting in four Lorentzians in the vicinity of ∼2700 cm^{-1}. The resultant 2*D* band is the combination of these four components and no longer represents a Lorentzian. Similarly, for trilayer graphene 15 different transitions are possible, and the 2*D* band consists of 15 Lorentzians in the vicinity of ∼2700 cm^{-1}.[16]

However, if interlayer coupling is weak, the splitting of electronic dispersion is negligible, and therefore the splitting of the Raman 2*D* band is also negligible. We note that weak interlayer coupling and the absence of splitting in the 2*D* Raman band are common features of CVD-grown MLGs and have been reported by many groups in the past.[15,16,19,20] Reference 44 employed Landau level spectroscopy to demonstrate weak interlayer coupling in graphene layers CVD-grown on Ni. The correlation between CPP-MR and 2*D* line shape as described before indicates that the observed large negative CPP-MR effect originates from the weakly coupled graphene layers.

The weak interlayer coupling and resulting (quasi) two-dimensional picture described above is valid when the nearest-neighbor interlayer coupling (or interlayer transfer energy t_c) is sufficiently small compared to thermal (k_BT) and disorder-induced (Γ) broadening. Since we have observed giant negative magnetoresistance even at the lowest temperature of 10 K for which $\Gamma \sim 30$ K,[45] clearly $t_c < 30$ K ≈ 2.6 meV. This matches reasonably well with ref 46, which calculated $t_c \sim 5$ meV for quasi two-dimensional carriers in graphite. For HOPG samples, on the other hand, $t_c \sim 0.39$ eV[14] $\gg k_BT$, Γ, and the above quasi two-dimensional picture does not hold for $T \leq 300$ K. The Raman 2*D* band of HOPG is also asymmetric with a pronounced shoulder peak (Figure 4a, Figure S8). Thus, no ILMR effect is expected in HOPG, which is consistent with our control experiments on the HOPG-like sample (Figure 4b) and previous work.[6]

As mentioned before, the presence of defects is negligible in the "defect-free region" of thick MLG samples grown on Ni foil (both homemade and purchased). For MLG-on-Ni, both fcc and hcp domains can form during CVD growth, depending on the adsorption sites of the carbon atoms.[47] According to ref 47, the grain boundaries between these domains are often "delaminated" from the substrate and MLG tends to bulge away from the substrate. These features allow matching of fcc and hcp domains by a continuous sheet of graphene, without formation of defects at the domain boundaries. In our MLG-on-Ni samples we have observed similar bulging features as shown in the Supporting Information (Figure S6). This is presumably the reason for absence of *D* peak in the "defect-free region" of our MLG-on-Ni samples. Thus, weak interlayer coupling is preserved in the "defect-free region" of MLG-on-Ni samples described in Figures 1 and 2, and in this region CPP charge transport primarily occurs via interlayer tunneling and not via conductive defect states.

The thin MLG samples (∼15−20 nm) as grown on Ni also show a symmetric 2*D* Raman peak (Figure 3c). However, unlike thicker specimens, these are accompanied by a defect (*D*) peak, and CPP transport is fundamentally different from the thicker samples (Figure 3). In these thinner samples CPP charge transfer primarily occurs via defect states instead of any interlayer tunneling. As a result, no large negative CPP-MR is observed in these thinner samples.

We have studied CPP-MR of MLG samples as grown on Cu (Supporting Information, section VII). Such devices have been studied by other groups in the past,[12] but no large negative CPP-MR (similar to Figure 2) was reported. Samples grown on copper typically show a symmetric 2*D* peak (Supporting Information, Figure S7a), and therefore a large negative CPP-MR is expected in these samples as well. However, the copper-grown MLG samples also exhibit a significant defect peak (∼1360 cm^{-1}, Figure S7a) in the Raman spectrum, which originates from the grain boundaries and also as a result of the fabrication process.[12,48] The edge states at the grain boundaries are known to be conductive[49] and can effectively short the neighboring graphene layers. In this case CPP charge transport will primarily occur via the conductive edge states instead of interlayer tunneling. This is presumably the reason for absence of large negative CPP-MR in Cu-grown samples. Transport through edge states and defects however results in a weak negative CPP-MR at low temperature due to weak localization, and this effect has been observed by us (Figure S7b) and is consistent with literature.[12]

Summarizing the above discussion, we conclude that for the samples in Figures 1 and 2 the graphene layers in the "defect-free region" (i.e., away from the Ni/MLG interface) are characterized by a distortionless 2*D* band and the absence of a *D* band in the Raman spectrum. Thus, in this region interlayer coupling is weak, and charge transfer via conductive edge states (defects) is absent. Due to weak interlayer coupling, CPP resistance is dominated by these weakly coupled layers, and a large zero-field CPP resistivity is observed compared to typical HOPG samples.[6] CPP charge transfer in these layers takes place only by interlayer tunneling and results in a large negative ILMR in the presence of an out-of-plane magnetic field. Thus, the primary role of the Ni substrate is to realize graphene layers that are weakly coupled and are not electrically shorted with each other via conductive edge states. Our CVD growth parameters (Supporting Information, section I) allow us to simultaneously satisfy both of these conditions.

Varying the growth parameters can give rise to strong interlayer coupling characterized by a split or HOPG-like 2*D* band in the Raman spectrum (Figures 4a, c). Similarly in the case of commercially available HOPG, interlayer coupling is strong as well (Supporting Information, Figure S8). The growth on Cu leads to the formation of defect states at grain boundaries (Figure S7), which effectively short neighboring graphene layers. In all of these cases no ILMR has been observed. We have also transferred the Ni-grown MLG on Au and Ni electrodes (patterned on a SiO_2/Si substrate) and have performed CPP-MR measurements (Supporting Information, section IX). As mentioned before, unlike as-grown MLG these transferred samples exhibit a shoulder in the 2*D* Raman band that arises as a result of the transfer process (Figure S2). Thus, interlayer coupling is adversely affected as a result of transfer,

dx.doi.org/10.1021/nl4030853 | Nano Lett. XXXX, XXX, XXX−XXX

and we have not observed any large negative CPP-MR but found weak positive CPP-MR instead (Supporting Information, Figures S9 and S10), which is consistent with prior studies.[6,12,14]

According to the interlayer tunneling theory,[34] interlayer conductivity σ_{zz} (which is proportional to the inverse of measured interlayer resistance R_{zz}) is proportional to the out-of-plane magnetic field $|B|$ and is given by

$$\sigma_{zz} = 2C\tau|B|\frac{t_c^2 ce^3}{\pi\hbar^3}$$

where τ is the characteristic lifetime associated with Landau level broadening (or relaxation time for in-plane scattering), t_c is the interlayer transfer energy estimated to be ~2 meV for weakly coupled graphene layers (as discussed earlier), c represents interlayer spacing (~0.342 nm for turbostratic graphite with weakly coupled graphene layers), e is the electronic charge and $\hbar$ is reduced Planck constant. It has been shown[34] that C is $\sim 1/k_BT$ for "high temperatures" for which $k_BT > t_c, \hbar/\tau$. This condition is satisfied at almost all temperatures (above ~30 K) considered in this work, and hence C can be equated to $1/k_BT$. Now since τ is expected to decrease with increasing temperature, we expect the slope of $\sigma_{zz} - |B|$ curve to decrease with increasing temperature.

To check the validity of this model, first we have fitted $1/R_{zz}$ as a function of B as shown in Figure 5. A clear linear fit is

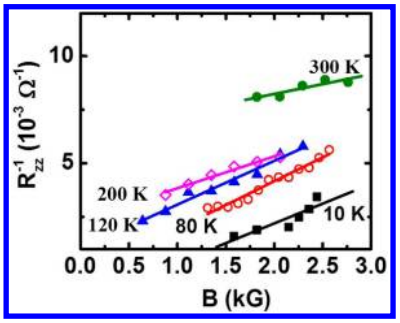

Figure 5. Inverse of CPP resistance (R_{zz}^{-1}) as a function of out-of-plane magnetic field (B) in the vicinity of the switching fields (B_{sw}). A linear trend is observed at all temperatures.

observed in the vicinity of ~2 kG, where the negative MR occurs. Further as mentioned above, the slope of $1/R_{zz}$ vs B is expected to decrease with increasing temperature, which is also consistent with Figure 5.

However, we note that this model is not valid in the low field regime (~0 kG) where inter Landau level mixing plays a dominant role.[35,36] This model also does not hold at high magnetic fields (>~ 3 kG) where additional level splitting (due to effects such as spin−orbit interactions) may become important. We note that a strong Rashba type splitting has been reported in graphene/Ni composites,[3] which can become further pronounced in the presence of high magnetic field. Such additional level splittings will clearly affect the high field CPP-MR. Such effects are not captured by the interlayer tunneling model described above. Additionally, strain in graphene layers can result in strong out-of-plane pseudomagnetic field (~300 T), which mimics the externally applied field and gives rise to pseudo Landau levels.[50] Stacking misorientations in graphene layers can result in strong in-plane pseudomagnetic field.[51] These effects may play a role in quantitative understanding of the observed MR effect.

The observed angle dependence of the CPP-MR response (Figure 2) is also consistent with the interlayer tunneling theory. As described before, in the $B \perp I$ configuration, classical Lorentz force bends carrier trajectory to the direction parallel to the MLG plane, which reduces interlayer tunneling probability and results in a positive MR. Such bending becomes less pronounced at higher temperatures due to thermal fluctuations. As a result, the positive CPP-MR effect weakens with increasing temperature as observed in Figure 2.

In Figure 2, the shape of the *low-field* MR response (± 2 kG range) is strongly dependent on temperature. At low temperatures (10−80 K) the low-field MR response is "smooth-topped" with gradual variation in the neighborhood of zero field, but at higher temperature (160 K, 250 K) the low-field MR response becomes "flat topped". This indicates that at higher temperature a competing *positive* (low-field) MR effect emerges that offsets the negative (low-field) MR and makes the net (low-field) MR flat-topped. At 300 K, the positive MR effect is quite dominant, and we see a weak net positive MR effect in the near vicinity of the zero field. As described below, the "interlayer tunneling" model mentioned above can be used to obtain a qualitative understanding of the temperature dependence of low-field MR curves.

According to the interlayer tunneling model, the low-field MR response results from a competition between the following two mechanisms: (a) interlayer tunneling between the zero-mode Landau levels, which gives rise to negative MR, and this effect becomes dominant as the magnetic field is increased due to an increase in Landau level degeneracy, and (b) a positive MR effect, which originates from inter-Landau level mixing due to thermal broadening.[35] The positive MR effect is only effective at a low field range and higher temperature, where inter-Landau level spacing is comparable to thermal broadening. In presence of inter-Landau level mixing, interlayer carrier transfer is not perpendicular to the plane, which results in a positive MR. We observed such effects for temperatures 160 and 250 K (Figures 2d, e), at which the positive MR effect offsets the negative MR effect in the vicinity of zero field and results in a flat-topped MR response near zero field. At 300 K (Figure 2f) the positive MR exceeds the negative MR, and hence we observe a small net positive MR near zero field. At 10, 30, and 80 K (Figures 2a, b, c) thermal broadening is negligible, which suppresses the positive MR effect, and only a negative MR is observed at low field.

Figure S11 (Supporting Information) shows the temperature dependence of the "switching field (B_{SW})" at which sharp drop in CPP resistance takes place due to the negative MR effect. In this plot B_{SW} is taken to be the field value at which resistance decreases to 50% of its zero-field value, and B_{SW} essentially demarcates the low field region from the high field region. We note that the switching field as defined above is not necessarily same as the "critical magnetic field" required to achieve "quantum limit".[34] As described before, the low field MR is a result of two competing processes, and the negative MR effect should be dominant when the inter Landau level mixing is not significant (but not necessarily zero). To reduce inter Landau level mixing, spacing between neighboring Landau levels should be made comparable (or larger) than thermal broadening of the Landau levels. Inter Landau level spacing increases with magnetic field,[38] and thermal broadening increases with temperature. Thus, at higher temperatures, negative MR will

dx.doi.org/10.1021/nl4030853 | *Nano Lett.* XXXX, XXX, XXX−XXX

manifest at a higher magnetic field. Thus, B_{sw} is expected to show an increasing trend with temperature. This is consistent with Figure S11.

In conclusion, we have observed a novel giant negative CPP-MR (>10^4%) in MLG as grown on Ni, which persists even at room temperature. The negative MR manifests in thick multilayer samples in which the Raman 2*D* peak does not exhibit any significant splitting (or HOPG-like distortion) and the *D* peak is absent. Such features have been realized by controlling the parameters of the CVD growth process. The observed data are qualitatively consistent with the "interlayer magnetoresistance" (ILMR) mechanism in which interlayer charge transfer occurs between the zero mode Landau levels of weakly coupled graphene layers. Due to the large MR value and its persistence at room temperature, this effect is expected to have commercial implications and encourage further research on MLG physics and MLG growth mechanisms on ferromagnetic substrates.

■ ASSOCIATED CONTENT

Supporting Information

Experimental details such as MLG growth, transfer, characterization of transferred MLG, etc. This material is available free of charge via the Internet at http://pubs.acs.org.

■ AUTHOR INFORMATION

Corresponding Author

*E-mail: spramani@ualberta.ca.

Notes

The authors declare no competing financial interest.

■ ACKNOWLEDGMENTS

This work has been supported by TRTech (formerly TRLabs) Disruptive Technology Challenge, NSERC, and SEE. We thank Mr. Rob Indoe at the National Institute for Nanotechnology (NINT) for help in sample preparation.

■ REFERENCES

(1) Chappert, C.; Fert, A.; Dau, F. N. V. *Nat. Mater.* **2007**, *6*, 813−823.

(2) Karpan, V. M.; Giovannetti, G.; Khomyakov, P. A.; Talanana, M.; Starikov, A. A.; Zwierzycki, M.; van den Brink, J.; Brocks, G.; Kelly, P. J. *Phys. Rev. Lett.* **2007**, *99*, 176602.

(3) Dedkov, Y. S.; Fonin, M.; Rüdiger, U.; Laubschat, C. *Phys. Rev. Lett.* **2008**, *100*, 107602.

(4) Novoselov, K. S.; Jiang, Z.; Zhang, Y.; Morozov, S. V.; Stormer, H. L.; Zeitler, U.; Maan, J. C.; Boebinger, G. S.; Kim, P.; Geim, A. K. *Science* **2007**, *315*, 1379−1379.

(5) Dean, C. R.; Young, A. F.; Cadden-Zimansky, P.; Wang, L.; Ren, H.; Watanabe, K.; Taniguchi, T.; Kim, P.; Hone, J.; Shepard, K. L. *Nat. Phys.* **2011**, *7*, 693−696.

(6) Kempa, H.; Esquinazi, P.; Kopelevich, Y. *Phys. Rev. B* **2002**, *65*, 241101.

(7) Zhi-Ming, W.; Ding-Yu, X.; Shi-Yuan, Z.; Qing-Yu, X.; VanBael, M.; You-Wei, D. *Chin. Phys. Lett.* **2007**, *24*, 199−202.

(8) Liu, Y.; Lew, W. S.; Sun, L. *Phys. Chem. Chem. Phys.* **2011**, *13*, 20208.

(9) Wu, X.; Li, X.; Song, Z.; Berger, C.; de Heer, W. A. *Phys. Rev. Lett.* **2007**, *98*, 136801.

(10) Tikhonenko, F. V.; Kozikov, A. A.; Savchenko, A. K.; Gorbachev, R. V. *Phys. Rev. Lett.* **2009**, *103*, 226801.

(11) Matis, B. R.; Bulat, F. A.; Friedman, A. L.; Houston, B. H.; Baldwin, J. W. *Phys. Rev. B* **2012**, *85*, 195437.

(12) Liao, Z.-M.; Wu, H.-C.; Kumar, S.; Duesberg, G. S.; Zhou, Y.-B.; Cross, G. L. W.; Shvets, I. V.; Yu, D.-P. *Adv. Mater.* **2012**, *24*, 1862−1866.

(13) Friedman, A. L.; Tedesco, J. L.; Campbell, P. M.; Culbertson, J. C.; Aifer, E.; Perkins, F. K.; Myers-Ward, R. L.; Hite, J. K.; Eddy, C. R.; Jernigan, G. G.; Gaskill, D. K. *Nano Lett.* **2010**, *10*, 3962−3965.

(14) Kopelevich, Y.; da Silva, R. R.; Pantoja, J. C. M.; Bratkovsky, A. M. *Phys. Lett. A* **2010**, *374*, 4629−4632.

(15) Reina, A.; Jia, X.; Ho, J.; Nezich, D.; Son, H.; Bulovic, V.; Dresselhaus, M. S.; Kong, J. *Nano Lett.* **2008**, *9*, 30−35.

(16) Malard, L. M.; Pimenta, M. A.; Dresselhaus, G.; Dresselhaus, M. S. *Phys. Rep.* **2009**, *473*, 51−87.

(17) Charlier, J.; Eklund, P.; Zhu, J.; Ferrari, A. In *Carbon Nanotubes*; Springer: Berlin/Heidelberg, 2008; Vol. *111*, pp 673−709.

(18) Kim, K. S.; Zhao, Y.; Jang, H.; Lee, S. Y.; Kim, J. M.; Kim, K. S.; Ahn, J.-H.; Kim, P.; Choi, J.-Y.; Hong, B. H. *Nature* **2009**, *457*, 706−710.

(19) Faugeras, C.; Nerrière, A.; Potemski, M.; Mahmood, A.; Dujardin, E.; Berger, C.; de Heer, W. A. *Appl. Phys. Lett.* **2008**, *92*, 011914−011914-3.

(20) Lenski, D. R.; Fuhrer, M. S. *J. Appl. Phys.* **2011**, *110*, 013720−013720-4.

(21) Ammar, M. R.; Rouzaud, J. N.; Vaudey, C. E.; Toulhoat, N.; Moncoffre, N. *Carbon* **2010**, *48*, 1244−1251.

(22) Ni, Z. h.; Wang, Y. y.; Yu, T.; Shen, Z. x. *arXiv* **2008**, 0810.2836.

(23) Blake, P.; Hill, E. W.; Neto, A. H. C.; Novoselov, K. S.; Jiang, D.; Yang, R.; Booth, T. J.; Geim, A. K. *Appl. Phys. Lett.* **2007**, *91*, 063124.

(24) Wang, X.; Chen, Y. P.; Nolte, D. D. *Opt. Express* **2008**, *16*, 22105−22112.

(25) Bodepudi, S.; Singh, A.; Pramanik, S. *Electronics* **2013**, *2*, 315−331.

(26) Matsubara, K.; Sugihara, K.; Tsuzuku, T. *Phys. Rev. B* **1990**, *41*, 969−974.

(27) Venugopal, G.; Jung, M.-H.; Suemitsu, M.; Kim, S.-J. *Carbon* **2011**, *49*, 2766−2772.

(28) Heo, J.; Chung, H. J.; Lee, S.-H.; Yang, H.; Seo, D. H.; Shin, J. K.; Chung, U.-I.; Seo, S.; Hwang, E. H.; Das Sarma, S. *Phys. Rev. B* **2011**, *84*, 035421.

(29) Oostinga, J. B.; Sacépé, B.; Craciun, M. F.; Morpurgo, A. F. *Phys. Rev. B* **2010**, *81*, 193408.

(30) Poumirol, J.-M.; Cresti, A.; Roche, S.; Escoffier, W.; Goiran, M.; Wang, X.; Li, X.; Dai, H.; Raquet, B. *Phys. Rev. B* **2010**, *82*, 041413.

(31) Bai, J.; Cheng, R.; Xiu, F.; Liao, L.; Wang, M.; Shailos, A.; Wang, K. L.; Huang, Y.; Duan, X. *Nat. Nanotechnol.* **2010**, *5*, 655−659.

(32) Wintterlin, J.; Bocquet, M.-L. *Surf. Sci.* **2009**, *603*, 1841−1852.

(33) Chae, S. J.; Güneş, F.; Kim, K. K.; Kim, E. S.; Han, G. H.; Kim, S. M.; Shin, H.-J.; Yoon, S.-M.; Choi, J.-Y.; Park, M. H.; Yang, C. W.; Pribat, D.; Lee, Y. H. *Adv. Mater.* **2009**, *21*, 2328−2333.

(34) Osada, T. *J. Phys. Soc. Jpn.* **2008**, *77*, 084711.

(35) Morinari, T.; Tohyama, T. *J. Phys. Soc. Jpn.* **2010**, *79*, 044708.

(36) Tajima, N.; Sugawara, S.; Kato, R.; Nishio, Y.; Kajita, K. *Phys. Rev. Lett.* **2009**, *102*, 176403.

(37) Tajima, N.; Sato, M.; Sugawara, S.; Kato, R.; Nishio, Y.; Kajita, K. *Phys. Rev. B* **2010**, *82*, 121420.

(38) Castro Neto, A. H.; Guinea, F.; Peres, N. M. R.; Novoselov, K. S.; Geim, A. K. *Rev. Mod. Phys.* **2009**, *81*, 109−162.

(39) Thomsen, C.; Reich, S. *Phys. Rev. Lett.* **2000**, *85*, 5214−5217.

(40) Saito, R.; Jorio, A.; Souza Filho, A. G.; Dresselhaus, G.; Dresselhaus, M. S.; Pimenta, M. A. *Phys. Rev. Lett.* **2001**, *88*, 027401.

(41) Narula, R.; Reich, S. *Phys. Rev. B* **2008**, *78*, 165422.

(42) Ferrari, A. C.; Meyer, J. C.; Scardaci, V.; Casiraghi, C.; Lazzeri, M.; Mauri, F.; Piscanec, S.; Jiang, D.; Novoselov, K. S.; Roth, S.; Geim, A. K. *Phys. Rev. Lett.* **2006**, *97*, 187401.

(43) Pimenta, M. A.; Dresselhaus, G.; Dresselhaus, M. S.; Cancado, L. G.; Jorio, A.; Saito, R. *Phys. Chem. Chem. Phys.* **2007**, *9*, 1276.

(44) Luican, A.; Li, G.; Reina, A.; Kong, J.; Nair, R. R.; Novoselov, K. S.; Geim, A. K.; Andrei, E. Y. *Phys. Rev. Lett.* **2011**, *106*, 126802.

(45) Giesbers, A. J. M.; Ponomarenko, L. A.; Novoselov, K. S.; Geim, A. K.; Katsnelson, M. I.; Maan, J. C.; Zeitler, U. *Phys. Rev. B* **2009**, *80*, 201403.
(46) Haering, R. R.; Wallace, P. R. *J. Phys. Chem. Solids* **1957**, *3*, 253−274.
(47) Lahiri, J.; Lin, Y.; Bozkurt, P.; Oleynik, I. I.; Batzill, M. *Nat. Nanotechnol.* **2010**, *5*, 326−329.
(48) Yu, Q.; Jauregui, L. A.; Wu, W.; Colby, R.; Tian, J.; Su, Z.; Cao, H.; Liu, Z.; Pandey, D.; Wei, D.; Chung, T. F.; Peng, P.; Guisinger, N. P.; Stach, E. A.; Bao, J.; Pei, S.-S.; Chen, Y. P. *Nat. Mater.* **2011**, *10*, 443−449.
(49) Acik, M.; Chabal, Y. J. *Jpn. J. Appl. Phys.* **2011**, *50*, 070101.
(50) Levy, N.; Burke, S. A.; Meaker, K. L.; Panlasigui, M.; Zettl, A.; Guinea, F.; Neto, A. H. C.; Crommie, M. F. *Science* **2010**, *329*, 544−547.
(51) He, W.-Y.; Su, Y.; Yang, M.; He, L. *Phys. Rev. B* **2014**, *89*, 125418.

dx.doi.org/10.1021/nl4030853 | *Nano Lett.* XXXX, XXX, XXX−XXX